

## NEUROSYSTEMS

# Ultrastructural characterization of the mesostriatal dopamine innervation in mice, including two mouse lines of conditional VGLUT2 knockout in dopamine neurons

Noémie Bérubé-Carrière,<sup>1</sup> Ginette Guay,<sup>1</sup> Guillaume M. Fortin,<sup>2</sup> Klas Kullander,<sup>3</sup> Lars Olson,<sup>4</sup> Åsa Wallén-Mackenzie,<sup>3</sup> Louis-Eric Trudeau<sup>2,5</sup> and Laurent Descarries<sup>1,5,6</sup>

<sup>1</sup>Department of Pathology and Cell Biology, Faculty of Medicine, C.P. 6128, Succursale Centre-Ville, Université de Montréal, Montréal, QC H3C 3J7, Canada

<sup>2</sup>Department of Pharmacology, Faculty of Medicine, Université de Montréal, Montréal, QC, Canada

<sup>3</sup>Department of Neuroscience, Unit of Developmental Genetics, Uppsala University, Uppsala, Sweden

<sup>4</sup>Department of Neuroscience, Karolinska Institutet, Stockholm, Sweden

<sup>5</sup>Groupe de Recherche sur le Système Nerveux Central, Université de Montréal, Montréal, QC, Canada

<sup>6</sup>Department of Physiology, Faculty of Medicine, Université de Montréal, Montréal, QC, Canada

**Keywords:** conditional *Vglut2* KO, diffuse transmission, electron microscopy, neostriatum, nucleus accumbens, tyrosine hydroxylase immunocytochemistry

## Abstract

Despite the increasing use of genetically modified mice to investigate the dopamine (DA) system, little is known about the ultrastructural features of the striatal DA innervation in the mouse. This issue is particularly relevant in view of recent evidence for expression of the vesicular glutamate transporter 2 (VGLUT2) by a subset of mesencephalic DA neurons in mouse as well as rat. We used immuno-electron microscopy to characterize tyrosine hydroxylase (TH)-labeled terminals in the core and shell of nucleus accumbens and the neostriatum of two mouse lines in which the *Vglut2* gene was selectively disrupted in DA neurons (cKO), their control littermates, and C57BL/6/J wild-type mice, aged P15 or adult. The three regions were also examined in cKO mice and their controls of both ages after dual TH–VGLUT2 immunolabeling. Irrespective of the region, age and genotype, the TH-immunoreactive varicosities appeared similar in size, vesicular content, percentage with mitochondria, and exceedingly low frequency of synaptic membrane specialization. No dually labeled axon terminals were found at either age in control or in cKO mice. Unless TH and VGLUT2 are segregated in different axon terminals of the same neurons, these results favor the view that the glutamatergic cophenotype of mesencephalic DA neurons is more important during the early development of these neurons than for the establishment of their scarce synaptic connectivity. They also suggest that, in mouse even more than rat, the mesostriatal DA system operates mainly through non-targeted release of DA, diffuse transmission and the maintenance of an ambient DA level.

## Introduction

The word ‘synapse’ was coined by Sherrington (1897) more than 50 years before synaptic junctions between central nervous system (CNS) neurons were first seen. It was meant to designate sites of functional contact between distinct neuronal entities. When electron microscopy revealed the presence of small areas of plasma membrane differentiation between neuronal elements, against which storage-like vesicles accumulated on the side of presumed transmitter release (Robertson, 1953; Palade & Palay, 1954), these junctional complexes came to be recognized as the hallmark of synapses (Peters & Palay, 1996). For many years, they were actually considered as the only site of chemical communication between CNS neurons. Transmitter

release would take place by exocytosis alongside presynaptic thickenings, and receptors for the transmitter would be confined to postsynaptic densities.

When CNS monoamine neurons were first demonstrated to be only partly synaptic (Descarries *et al.*, 1975, 1977), in the sense that many of their axon varicosities, terminals or boutons did not display a synaptic membrane specialization, it was logical to envisage the possibility that chemical transmission from these varicosities be widespread (diffuse or volume transmission) through activation of extrasynaptic transmitter receptors (Beaudet & Descarries, 1976). Moreover, because the presence of junctional complexes implied some fixity and permanence in the structural relationship between pre- and postsynaptic elements, the converse was suggestive of some flexibility and mobility of the releasing sites with respect to their immediate microenvironment (Descarries *et al.*, 1975).

In this context, and in view of the increasing use of this species in contemporary neuroscience, the almost total lack of knowledge about

*Correspondence:* Laurent Descarries, <sup>1</sup>Department of Pathology and Cell Biology, as above.

E-mail: laurent.descarries@umontreal.ca

Received 19 October 2011, revised 2 December 2011, accepted 8 December 2011

the ultrastructural morphology of the mesostriatal innervation in mouse, and notably the junctional vs. nonjunctional nature of its axon terminals, is surprising. The sole exception is the report of Triarhou *et al.* (1988), describing the cytological relationships of tyrosine hydroxylase (TH)-immunolabeled axon terminals in the laterodorsal neostriatum of two normal mice, as part of a broader group of investigations in heterozygous and homozygous Weaver mutants. Detailed information in the mouse is especially desired in view of the increasing use of genetically modified mice for studies of the dopamine (DA) system (e.g., Birgner *et al.*, 2009; Stuber *et al.*, 2010) and, notably, the growing evidence that a subpopulation of mesencephalic DA neurons expresses the type 2 vesicular glutamate transporter (*Vglut2*) in both mouse and rat (Dal Bo *et al.*, 2004, 2008; Kawano *et al.*, 2006; Yamaguchi *et al.*, 2007; Mendez *et al.*, 2008; Stuber *et al.*, 2010). Moreover, recent optogenetic studies have shown that activation of mesencephalic DA neurons evokes glutamate-mediated synaptic events in the nucleus accumbens but not the neostriatum of adult mice (Stuber *et al.*, 2010; Tecuapetla *et al.*, 2010), suggesting that the glutamatergic cophenotype of a subset of mesencephalic DA neurons might not regress with age in this species, contrary to the situation in rats (Bérubé-Carrière *et al.*, 2009; see also Moss *et al.*, 2011).

In this study, we used immuno-electron microscopy after TH immunolabeling to analyze the fine structural characteristics of the mesostriatal DA innervation in the ventral and dorsal striatum of two lines of conditional KO (cKO) mice in which the *Vglut2* gene was specifically disrupted in DA neurons, their respective controls and wild-type mice. Mice aged P15 or adult were examined to detect morphological differences that might be associated with maturation. Doubly TH- and VGLUT2-immunolabeled material from control and cKO mice of both ages was also examined, to search for dually labeled terminals in the controls. Major differences were not observed between regions, ages and genotypes, and no dually labeled terminals were found. Nonetheless, the bulk of the observations provide new insights into the role of the glutamatergic cophenotype of mesencephalic DA neurons, as well as the functional properties of the mesostriatal DA system.

## Materials and methods

### Animals

All procedures involving animals and their care were conducted in strict accordance with the *Guide to care and use of experimental animals* (Ed. 2) of the Canadian Council on Animal Care, as well as the guidelines of Swedish regulation and European Union Legislation. The experimental protocols were approved by the Comité de déontologie pour l'expérimentation sur des animaux (CDEA) of the Université de Montréal, and by the Uppsala animal ethical committee. Housing was at a constant temperature (21 °C) and humidity (60%), under a fixed 12-h light–dark cycle and free access to food and water.

Two lines of *Vglut2*<sup>f/f</sup>;DAT-cre cKO mice and their littermate controls were used, in addition to wild-type mice (C57BL/6/J from Charles River, Saint-Constant, QC, Canada). The first line of cKOs (Upp) was generated in Uppsala (Sweden), according to Birgner *et al.* (2009). In brief, transgenic mice in which *Cre* was specifically expressed in cells expressing the DA transporter DAT (*DAT-Cre* of mixed C57BL/6/J and Sv129 background; Ekstrand *et al.*, 2007) were mated with *Vglut2*<sup>f/f</sup> mice (mixed C57BL/6/J and Sv129 background; Wallén-Mackenzie *et al.*, 2006), and the colony maintained by breeding *Vglut2*<sup>f/+</sup>;DAT-cre with *Vglut2*<sup>f/f</sup> mice, to produce *Vglut2*<sup>f/f</sup>;DAT-cre cKO and *Vglut2*<sup>f/f</sup> control mice. The second line (Mtl) was produced in Montreal (Canada), as described in detail in a

forthcoming publication by G.M. Fortin, M.J. Bourque, J.A. Mendez, D. Leo, K. Nordenankar, C. Birgner, E. Arvidsson, V.V. Rymar, N. Bérubé-Carrière, L. Descarries, A.F. Sadikot, Å. Wallén-Mackenzie & L.É. Trudeau. *DAT-Cre* transgenic mice (129/Sv/J background; Zhuang *et al.*, 2005) were mated with *Vglut2*<sup>f/f</sup> mice (mixed 129/Sv/J-C57BL/6/J background; Tong *et al.*, 2007), and the colony maintained by breeding *Vglut2*<sup>f/+</sup>;DAT-cre mice with *Vglut2*<sup>f/f</sup> mice to produce *Vglut2*<sup>f/f</sup>;DAT-cre cKO and *Vglut2*<sup>f/+</sup>;DAT-cre control mice. In all experiments, only male mice were used to avoid potential confounding effects of gender.

### Antibody characterization

As in our previous study (Bérubé-Carrière *et al.*, 2009), the Clone TH-2 (T1299) from Sigma was used to detect TH. This monoclonal anti-TH antibody produced in mouse recognizes an epitope (amino acids 9–16) present in the N-terminal region of both rodent and human TH (Haycock, 1993). Its specificity for DA neurons was demonstrated not only by the topographic distribution of immunoreactive TH cell bodies and axon terminals in the different brain regions examined (e.g. Fig. 1), but also by their near total disappearance from mesencephalon and striatum after neonatal 6-OHDA lesion (Bérubé-Carrière *et al.*, 2009). The polyclonal anti-VGLUT2 antibody (Synaptic Systems, Göttingen, Germany) was raised in rabbit against a Strep-Tag fusion protein from the C-terminal domain of the predicted sequence (amino acids 510–582) of rat VGLUT2 (Takamori *et al.*, 2001). The immu-

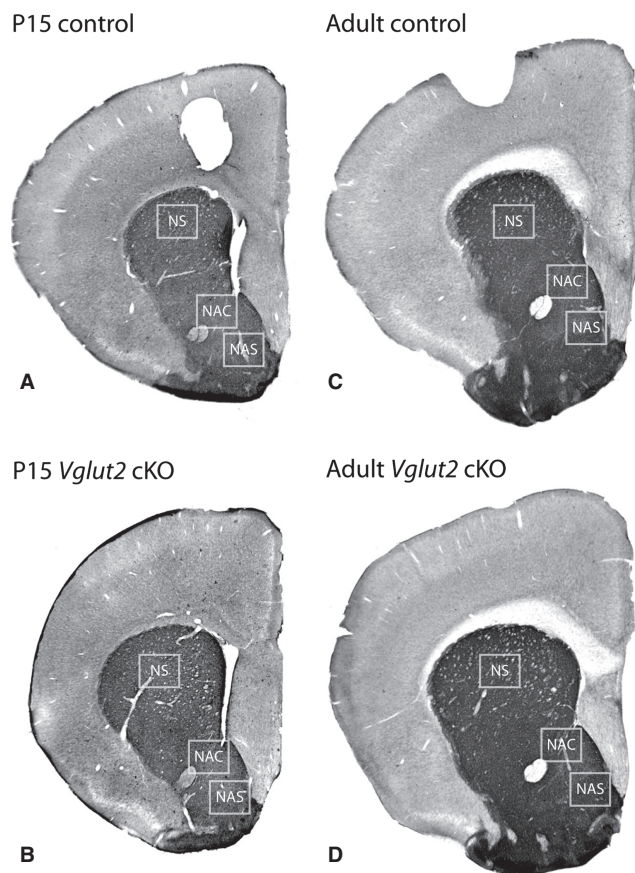


FIG. 1. Regions of neostriatum (NS) and nucleus accumbens core (NAC) and shell (NAS) sampled for electron microscopy. These sections across the striatum of (A and B) P15 and (C and D) adult (A and C) control and (B and D) cKO mice (Mtl) were processed for TH immunocytochemistry with the peroxidase–DAB technique.

nocytochemical specificity of this particular antibody has been demonstrated by Western blot analysis of homogenized rat brains and/or crude synaptic vesicle fractions from rat brain, in which a single broad band slightly above 60 kDa was found, and by pre-adsorption experiments with the GST fusion protein used as immunogen, in which the immunostaining of rat brain sections was completely eliminated (Takamori *et al.*, 2001; Persson *et al.*, 2006; Zhou *et al.*, 2007). This antibody has been previously used in combined immunocytochemical and *in situ* hybridization experiments to detect *Vglut2* mRNA in rat mesencephalic DA neurons (Kawano *et al.*, 2006), as well as for double TH and VGLUT2 immunolabeling of axon terminals in rat striatum at the electron microscopic level (Dal Bo *et al.*, 2008; Descarries *et al.*, 2008; Bérubé-Carrière *et al.*, 2009).

#### Single TH immunolabeling for light and electron microscopy

After deep anesthesia with sodium pentobarbital (80 mg/kg *i.p.*), immature (P15) and adult (70- to 90-day-old) mice were fixed by intracardiac perfusion of a solution of 3% acrolein in 0.1 M phosphate buffer (PB; pH 7.4; 50 mL for P15 mice, 100 mL for adult mice), followed by 4% PFA in the same buffer (100 mL for P15 mice, 150 mL for adult mice) – five cKO (two Upp and three Mtl) and five littermate controls (two Upp and three Mtl) at P15, and six adult cKO (three Upp and three Mtl) and their littermate controls (three Upp and three Mtl). An additional experiment was also carried out in two adult wild-type mice, in which 200 mL of 3% glutaraldehyde and 2.5% PFA in 0.1 M cacodylate buffer (pH 7.4) was perfused as primary fixative. In all cases, the brain was removed, post-fixed by immersion for 1 h in the PFA solution at 4 °C, and washed in phosphate-buffered saline (PBS; 0.9% NaCl in 50 mM PB, pH 7.4). Fifty-micrometre-thick transverse sections across the striatum (between stereotaxic levels 1.18 and 1.54 mm anterior to bregma in Franklin & Paxinos (2008)) were then cut in PBS with a vibrating microtome (VT100S; Leica Microsystems), immersed in 0.1% sodium borohydride (Sigma) in PBS for 30 min at room temperature, and washed in this buffer before immunocytochemical processing.

As already described in detail (Bérubé-Carrière *et al.*, 2009), sections intended for light microscopy were sequentially incubated in blocking solution containing 0.1% Triton X-100 (1 h), mouse monoclonal anti-TH antibody diluted 1 : 1000 (24 h), biotinylated goat antimouse IgGs (Jackson Immunoresearch) diluted 1 : 1000 (1.5 h), a 1 : 1000 solution of horseradish peroxidase (HRP)-conjugated streptavidin (Jackson Immunoresearch; 1 h), and 3,3'-diaminobenzidine tetrahydrochloride (0.05% DAB; Vector) and 0.005% hydrogen peroxide (2–3 min).

Sections intended for electron microscopy were similarly processed except for the omission of Triton X-100 in the blocking solution. Once immunostained, they were osmicated for 1 h in 1% OsO<sub>4</sub>, dehydrated in a graded series of ethanol, and flat-embedded in Durcupan resin (Sigma) between two sheets of Aclar plastic (EMS, Hatfield, PA, USA). After polymerization, the areas of interest were excised from the Aclar sheets and glued at the tip of resin blocks. Ultrathin (silver-gold) sections were then cut from the surface of the blocks, stained with Reynold's lead citrate and examined by electron microscopy (Philips CM100).

#### Dual TH–VGLUT2 immunolabeling for electron microscopy

Sections were processed as above, except for incubation for 24 h at room temperature in a 1 : 500 dilution of both primary TH and VGLUT2 antibodies. After rinses in PBS, they were then placed overnight, at room temperature, in a 1 : 50 dilution of donkey antirabbit IgGs conjugated to 0.8 nm colloidal gold particles (Aurion, Netherlands), and treated with

either the IntenSE kit (Amersham, Oakville, ON, Canada) or the HQ Silver kit (Nanoprobes, NY, USA) to increase the size of immunogold particles. The immunogold-labeled sections were then processed for TH with the immunoperoxidase technique, as above.

Immunocytochemical controls included double immunocytochemical processing, but without either one or both primary antibodies. Only the expected single labeling was then observed after omitting one of the primary antibodies, and no labeling was seen in the absence of both of them.

#### Quantitative analysis of TH-immunolabeled material

After single TH immunolabeling for electron microscopy, the nucleus accumbens core (NAC), nucleus accumbens shell (NAS) and neostriatum (NS) were examined in each of the 22 mice (P15 – five cKO and five control; adult – six cKO and six control) fixed by primary fixation of acrolein, the NAS in three mice (Mtl) of each of these four groups, and the NAC only in the two wild-type adult mice fixed with the glutaraldehyde–formaldehyde mixture. In every region of each mouse, at least 25 electron micrographs were taken at a working magnification of 15 000 $\times$ , within a narrow area of a thin section < 10  $\mu$ m away from the tissue–resin border. The film negatives were scanned (Epson Perfection 3200), converted into positive pictures, and adjusted for brightness and contrast with Adobe Photoshop, before printing at a final magnification of 37 500 $\times$ .

Most immunolabeled profiles could then be positively identified as axon varicosities, *i.e.*, axon dilations (> 0.25  $\mu$ m in transverse diameter) containing aggregated small vesicles and often one or more mitochondria, and displaying or not a synaptic membrane specialization (junctional complex). Using the public-domain Image J processing software from NIH, all axon varicosity profiles showing a distinct contour were measured for area, long (L) and short (s) axes and mean diameter (L + s/2), and then classified as showing or not a synaptic junction, *i.e.* a localized straightening and thickening of apposed plasma membranes on either side of a slightly widened extracellular space. The length of junctional complexes was measured and the synaptic targets identified, and the synaptic frequency observed in single thin sections was extrapolated to the whole volume of varicosities by means of the stereological formula of Beaudet & Sotelo (1981), which takes into account the average size of varicosity profiles, the average length of visible junctions and the thickness of the sections to calculate the probability of seeing the junction if one is made by every varicosity.

In total, 1135 TH-immunolabeled axon terminals were thus examined in the P15 (550 in control, 585 in cKO), and 1451 in the adult mice (709 in control, 742 in cKO; see Tables 1 and 2 for numbers examined in the different regions). In each control and in cKO mice of both ages, the number of axon terminals examined in every region was almost the same. In the two wild-type adult mice fixed by perfusion of the glutaraldehyde–paraformaldehyde mixture, 115 terminals were examined.

#### Electron microscopic examination of TH–VGLUT2 immunolabeled material

After dual TH–VGLUT2 immunolabeling, the three areas of interest were examined in thin sections from the 12 cKO (Mtl) mice and their controls processed for single TH immunolabeling plus one additional mouse in each group, giving a total of 16 mice. In every region of each mouse, 10–26 electron micrographs were obtained as above, which allowed for the examination of a total of 969 electron micrographs and a thin-section surface of 48 450  $\mu$ m<sup>2</sup> (see Table S1 for details and the number of labeled axon terminals visualized in

TABLE 1. DA axon terminals in the nucleus accumbens core and shell of immature (P15) and mature (P70-90), control and *Vglut2* cKO mice

	<i>n</i>	No.	Dimensions			Synaptic incidence		
			Mean dia. ( $\mu\text{m}$ )	Area ( $\mu\text{m}^2$ )	Mitochondria (%)	Single section (%)	Junction length ( $\mu\text{m}$ )	Whole varicosity (%)
NAC								
P15								
Control	5	182	0.47 $\pm$ 0.02	0.19 $\pm$ 0.02	27 $\pm$ 2	5 $\pm$ 2	0.20 $\pm$ 0.01	11 $\pm$ 3
cKO	5	210	0.47 $\pm$ 0.03	0.18 $\pm$ 0.02	36 $\pm$ 2	3 $\pm$ 1	0.22 $\pm$ 0.01	7 $\pm$ 2
P70-90								
Control	6	268	0.48 $\pm$ 0.01	0.20 $\pm$ 0.01	37 $\pm$ 3	3 $\pm$ 1	0.26 $\pm$ 0.03	6 $\pm$ 2
cKO	6	235	0.48 $\pm$ 0.01	0.20 $\pm$ 0.01	34 $\pm$ 4	4 $\pm$ 1	0.20 $\pm$ 0.01	8 $\pm$ 2
NAS								
P15								
Control	3	115	0.44 $\pm$ 0.02	0.16 $\pm$ 0.02	37 $\pm$ 9	3 $\pm$ 1	0.24 $\pm$ 0.05	5 $\pm$ 1
cKO	3	122	0.48 $\pm$ 0.04	0.21 $\pm$ 0.03	46 $\pm$ 2	2 $\pm$ 1	0.28 $\pm$ 0.03	5 $\pm$ 3
P70-90								
Control	3	162	0.45 $\pm$ 0.04	0.17 $\pm$ 0.02	48 $\pm$ 2	1 $\pm$ 1	0.16	2 $\pm$ 2
cKO	3	190	0.39 $\pm$ 0.02	0.14 $\pm$ 0.01	43 $\pm$ 5	1 $\pm$ 1	0.18	2 $\pm$ 1

*n*, number of mice; No., number of axon terminals examined. Mean  $\pm$  SEM from the number of mice. In this and the following table, the stereological formula of Beaudet & Sotelo (1981) was used to extrapolate the synaptic incidence for whole varicosities from the percentage of varicosity profiles showing a junction in single sections (details in Materials and Methods).

TABLE 2. DA axon terminals in the NS of immature (P15) and mature (P70-90) control and *Vglut2* cKO mice

	<i>n</i>	No.	Dimensions			Synaptic incidence		
			Mean dia. ( $\mu\text{m}$ )	Area ( $\mu\text{m}^2$ )	Mitochondria (%)	Single section (%)	Junction length ( $\mu\text{m}$ )	Whole varicosity (%)
P15								
Control	5	253	0.48 $\pm$ 0.02	0.20 $\pm$ 0.02	35 $\pm$ 2	5 $\pm$ 1	0.20 $\pm$ 0.01	12 $\pm$ 2
cKO	5	253	0.45 $\pm$ 0.02	0.19 $\pm$ 0.01	31 $\pm$ 6	3 $\pm$ 1	0.22 $\pm$ 0.04	7 $\pm$ 2
P70-90								
Control	6	279	0.48 $\pm$ 0.01	0.19 $\pm$ 0.01	42 $\pm$ 3	1 $\pm$ 1	0.14	3 $\pm$ 3
cKO	6	317	0.49 $\pm$ 0.01	0.20 $\pm$ 0.01	43 $\pm$ 3	1 $\pm$ 1	0.16 $\pm$ 0.02	2 $\pm$ 1

*n*, number of mice; No., number of axon terminals examined. Mean  $\pm$  SEM are from the number of mice indicated.

each region and each group). In tissue areas closest to the tissue–resin border there was obvious background labeling, in the form of dispersed silver-intensified gold particles. However, no attempt was made to subtract this nonspecific labeling for analysis of the results because the VGLUT2 immunolabeling of axon varicosities was very strong, and no TH-positive varicosities ever displayed three or more immunogold particles, except for a single profile of exceptionally large size, on which three immunogold particles were seen (see Fig. 6A).

### Statistics

Statistical analyses were performed in Prism 5 (GraphPad, La Jolla, CA, USA). One-way ANOVA and unpaired Student's *t*-tests were used to assess statistical significance. Results are presented as mean values  $\pm$  SEM. *P*-values below 0.05 were considered statistically significant.

### Results

#### Light microscopic visualization of striatal TH-immunostained innervation

In sections processed for light microscopic immunocytochemistry after TH-labeling with the immunoperoxidase–DAB technique, the

expected very dense labeling of the DA innervation was observed throughout the ventral and dorsal striatum of control as well as cKO mice (Fig. 1). In such 50- $\mu\text{m}$ -thick sections permeabilized with Triton X-100 and immunostained throughout their full thickness, this confluent labeling precluded any quantitative assessment of the number of axon varicosities in cKO vs. control mice.

#### Ultrastructural features of TH-immunoreactive varicosities

Immunoreactive axon varicosities (terminals) were readily identified as such in single thin sections for electron microscopy from material immunolabeled for TH only (Figs 2–5). Irrespective of the region (NAC, NAS and NS) and experimental group examined, these axon terminals were relatively small, generally round or oblong in shape but sometimes irregular in contour, and filled with small, round or ovoid synaptic vesicles, often accompanied by one or more mitochondria (Figs 2–5). Larger varicosity profiles were also observed (e.g. Figs 3D and 4E), but were relatively uncommon. The immunoperoxidase–DAB labeling was in the form of a more or less dense, fine precipitate, often outlining the small vesicles or mitochondria and the plasma membrane of varicosities. In many instances, a varicosity profile could be seen emerging from its parent unmyelinated axon (Figs 2B and 3C), in which case small vesicles were also present within the axon proper. It was not uncommon to

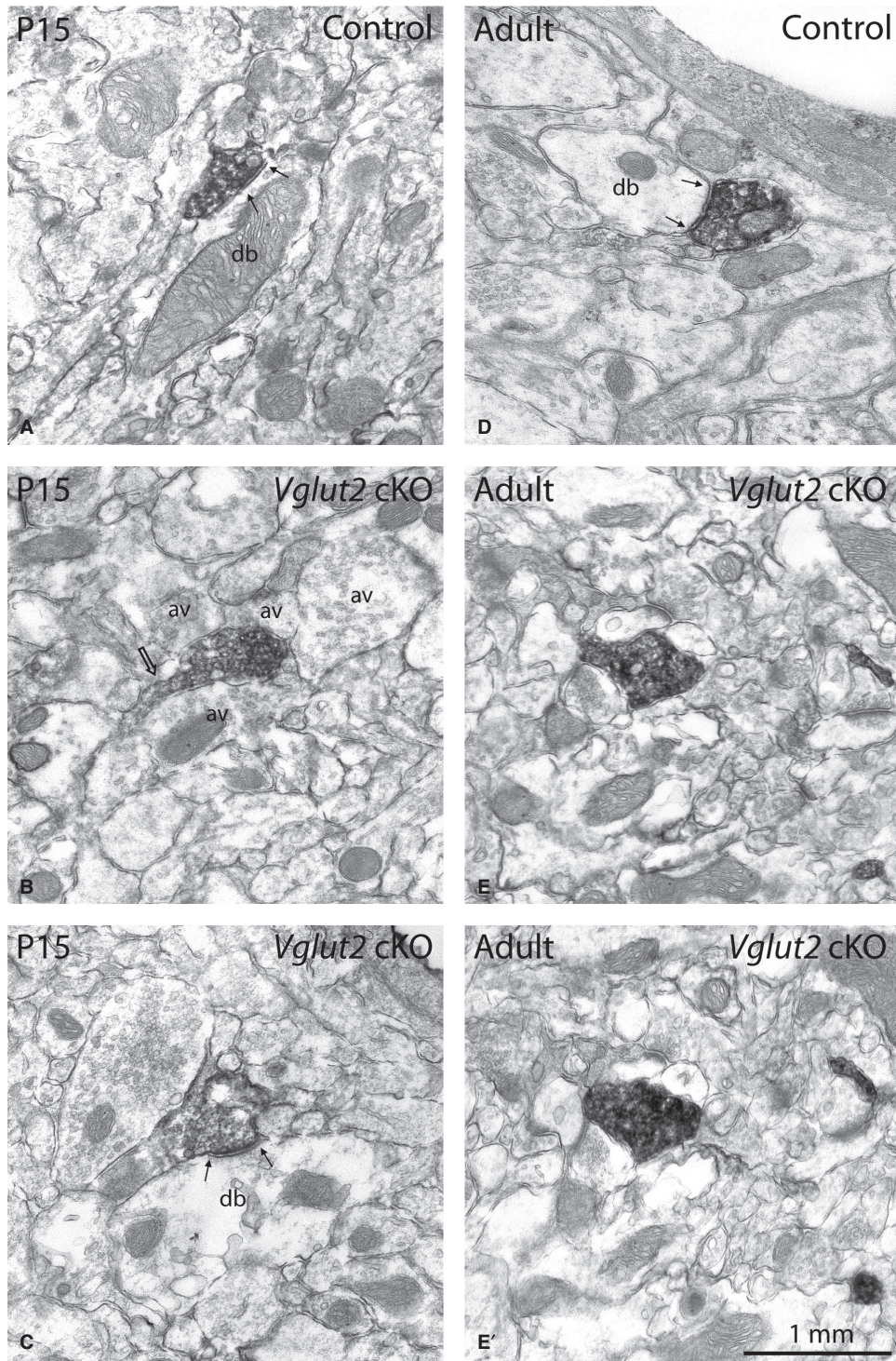


FIG. 2. DA terminals from the NAC in P15 or adult control and *Vglut2* cKO mice. As illustrated in this and the following figures, the TH-immunolabeled terminals (varicosities) in NAC (Figs 2 and 5) and NAS (Fig. 3), as well as in NS (Fig. 4), share similar ultrastructural features, whether in control or *Vglut2* cKO mice of both ages (see also Tables 1 and 2). These varicosities are relatively small, generally round or ovoid in shape, filled with small vesicles and associated or not with mitochondria, and the vast majority are without apparent synaptic membrane specialization (junctional complex). (A, C and D) Rare examples of TH-labeled synaptic varicosities, most of which form small, symmetrical junctions (between small arrows) with dendritic branches (db). (B, E and E') More typical examples of asynaptic terminals. In B, the labeled varicosity is seen emerging from its parent thin unmyelinated axon (open arrow), and it is directly apposed to several other unlabeled varicosities (av). E and E' are two sections across the same labeled terminal, neither of which displays a synaptic membrane specialization. A and D are from *Vglut2*<sup>f/+;DAT-cre</sup> and *Vglut2*<sup>f/f</sup> controls, respectively, whereas C is from a cKO (Mtl) and B, E and E' from cKO (Upp) mice. Tissue primarily fixed by perfusion of acrolein. Scale bar (in E'), 1  $\mu$ m.

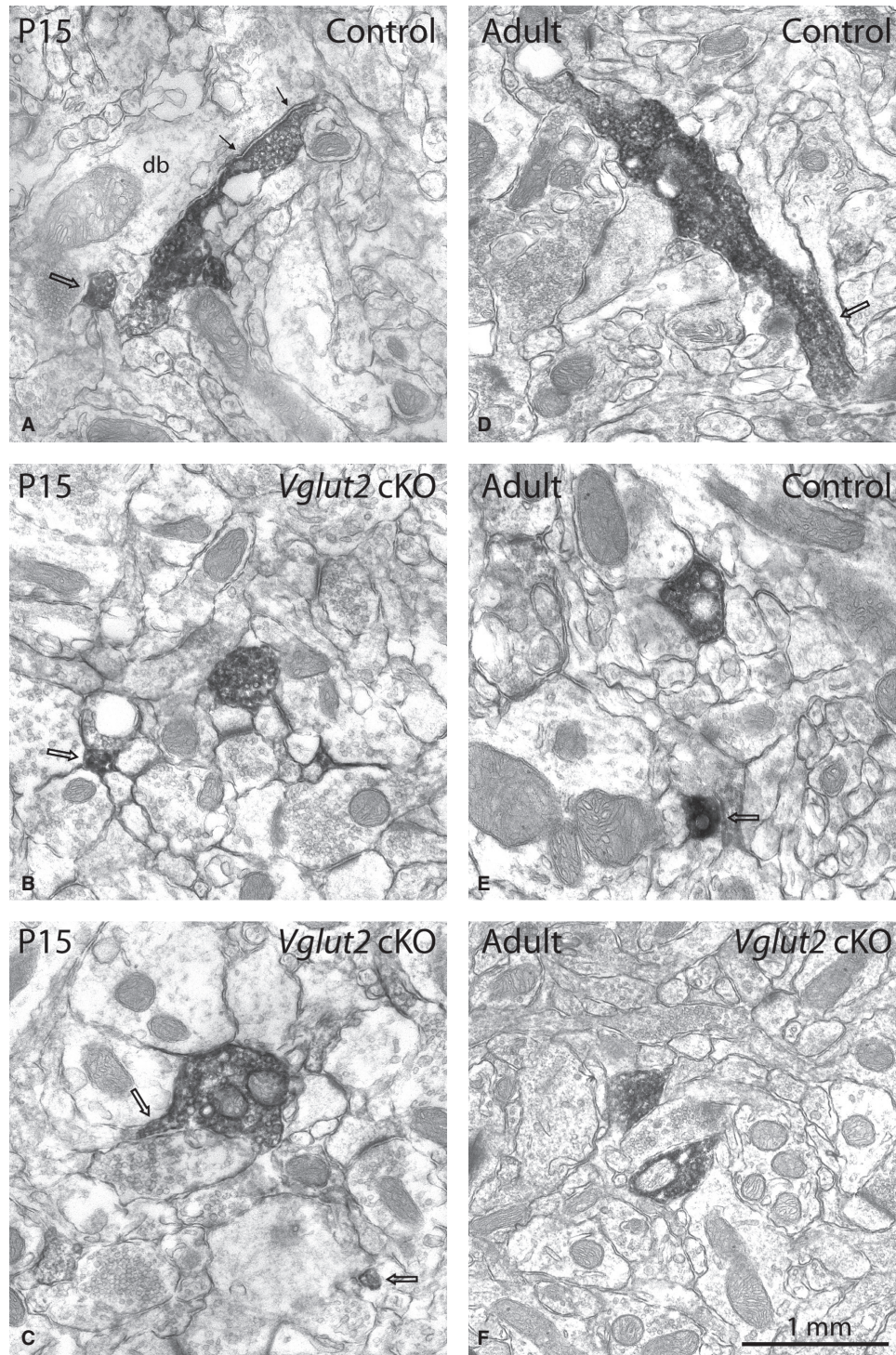


FIG. 3. DA terminals from the NAS in P15 or adult control and *Vglut2* cKO mice. These electron micrographs from the NAS (control or *Vglut2* cKO, Mtl) further illustrate ultrastructural characteristics of mesostriatal DA terminals in the mouse. (A) Two varicosities, along the same axon, are juxtaposed with a dendritic branch (db), with which the upper one forms a relatively wide symmetrical synapse (between small arrows). (B–F) All labeled terminals appear to be asynaptic. In A, B, C, and E, intervaricose axon segments are designated by open arrows. In D, the varicosity appears to be larger than average and its parent axon (open arrow) contains small vesicles in its narrow as well as dilated portion. Tissue primarily fixed by perfusion of acrolein. Scale bar (in F), 1  $\mu$ m.

find TH-labeled varicosities lying very close (Fig. 3F) or juxtaposed to one another (Fig. 5C), or almost in continuity along the same axon (Figs 3A,D and 4E).

All morphological parameters of the TH-labeled varicosities in each region and both ages were initially analyzed separately for the two types of cKO mice and their respective littermate controls (see

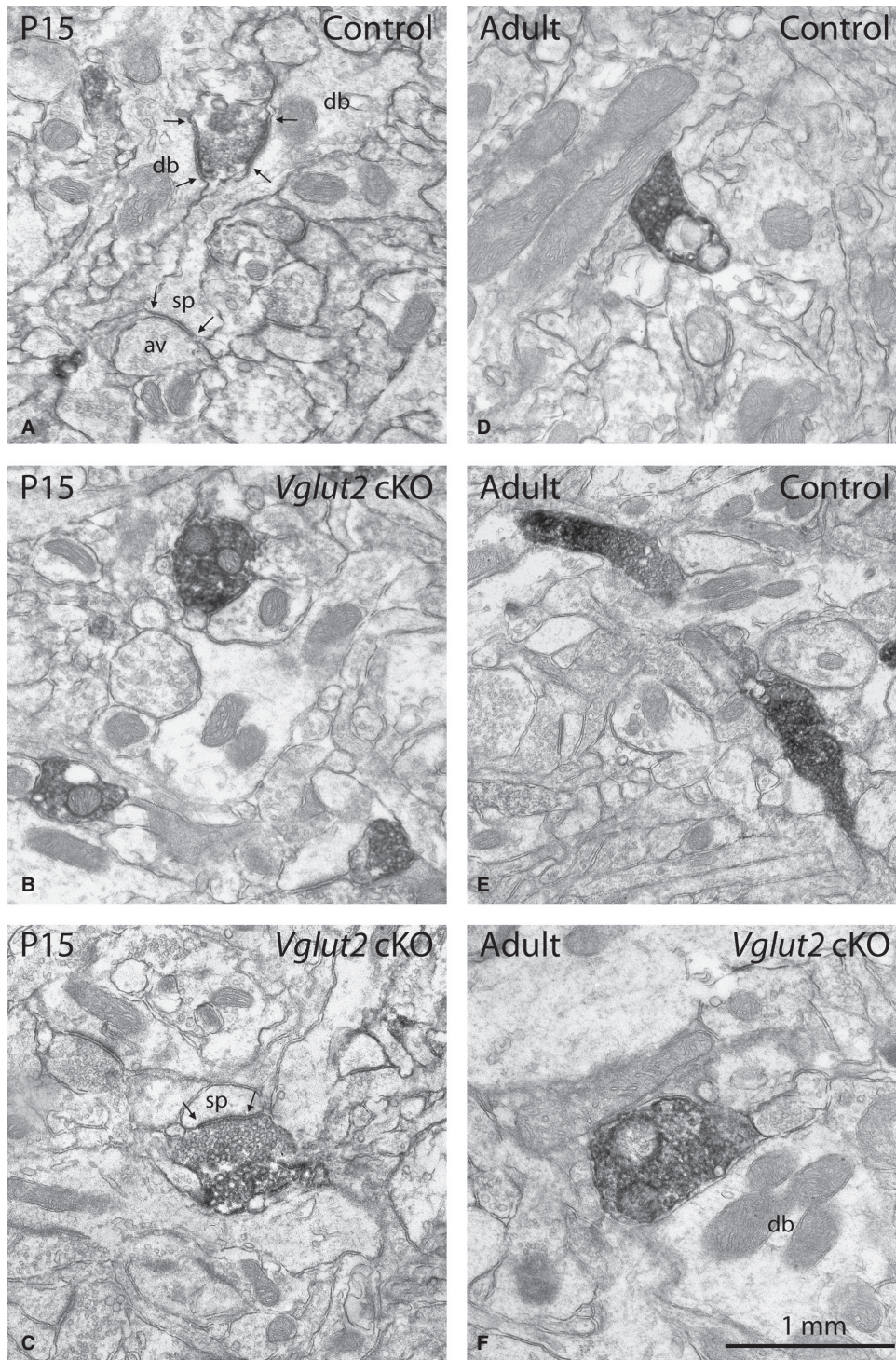
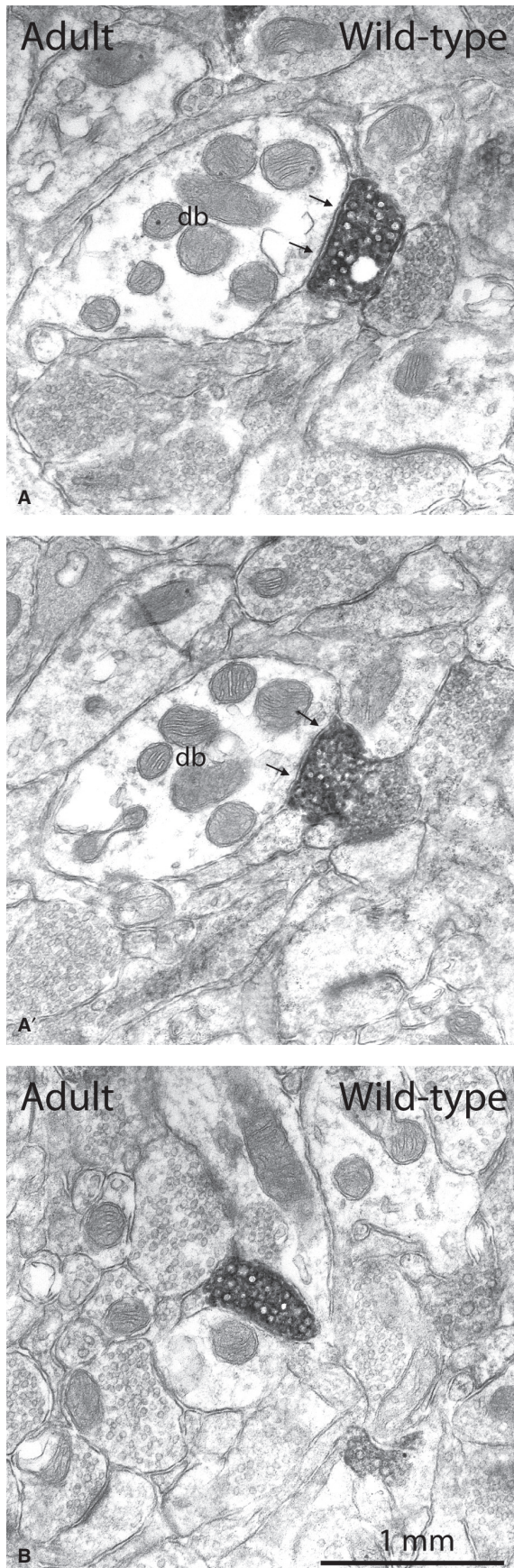


FIG. 4. DA terminals from the neostriatum in P15 or adult control and *Vglut2* cKO mice. (A) The TH-labeled varicosity is truly exceptional, as it displays not only one but two synaptic junctions (between small arrows) made with distinct dendritic branches (db). The synapse on the right is on the neck of a spine (sp) which arises from the upper dendritic branch. This spine is contacted synaptically on its head by another axon varicosity (av), unlabeled. (C) Rare occurrence of a labeled varicosity in synaptic contact (between small arrows) with a dendritic spine (sp). In this case, the junction looks rather asymmetrical. Note that this synaptic labeled varicosity is itself juxtaposed with another labeled varicosity profile, which is not entirely uncommon. (B, D, E and F) Representatives of the large majority of asynaptic labeled terminals. In B, the presence of three varicosity profiles within the same field reflects the high density of innervation. In E, the two elongated profiles presumably belong to the same axon, again illustrating the very short interval between such varicosities. F is another example of a relatively large TH-labeled varicosity. A, E and D are from *Vglut2*<sup>f/+;DAT-cre</sup> and *Vglut2*<sup>f/f</sup> controls, respectively, whereas B is from a cKO (Mtl) and C and F from cKO mice. Tissue primarily fixed by perfusion of acrolein. Scale bar (in F), 1 μm.



Tables S2 and S3). However, because there were no statistically significant differences in dimensions, percentage with mitochondria or synaptic incidence between any of these subgroups, data from the two cKO lines were pooled for presentation, as were the data from their respective controls (Tables 1 and 2).

Tables 1 and 2 give the results of this morphometric analysis for the three regions, P15 and adult and control or cKO mice. Overall, the diameter of TH-labeled varicosity profiles ranged between 0.39 and 0.49  $\mu\text{m}$ , averaging  $0.47 \pm 0.01 \mu\text{m}$ . This corresponded to an area of 0.14–0.21  $\mu\text{m}^2$  ( $0.19 \pm 0.01 \mu\text{m}^2$  on average), as individually calculated by Image J. The proportion of labeled varicosities containing one or more mitochondria ranged from 27 to 48% (total average,  $38 \pm 2\%$ ). In contrast to unlabeled varicosity profiles in their immediate surrounding, only a very small proportion of the TH-labeled profiles from each region exhibited a morphologically defined area of synaptic membrane specialization in all experimental groups (P15 or adult mice, cKO mice and their controls, adult wild-type mice). The few junctions that were observed (65 in total) were mostly symmetrical (e.g., Figs 2A,C,D, 3A, 4A,C and 5A–A') and made either with dendritic branches (Figs 2A,C,D, 3A, 4A and 5A–A'), or more rarely with spines (Fig. 4C). Although some labeled-varicosity profiles were occasionally found in direct apposition to neuronal cell bodies, no morphologically defined axosomatic synapses were seen.

Overall, the proportion of TH-labeled varicosities observed to form a synaptic junction in our single thin sections ranged from 0.5 to 5.1%, averaging  $2.6 \pm 0.5\%$ . The mean length of junctions formed by these few synaptic varicosities ranged from 0.14 to 0.28  $\mu\text{m}$ , averaging  $0.20 \pm 0.01 \mu\text{m}$ , again without significant difference between subgroups (Table S4). According to the formula of Beaudet & Sotelo (1981), this would represent a synaptic incidence ranging from 1.1 to 11.8% and averaging  $5.6 \pm 1\%$ , as extrapolated to the whole volume of varicosities. These percentages have to be regarded with caution, however, as they were calculated by means of a probabilistic formula applied to a very small number of occurrences.

Overall, there were more synapses made with dendritic branches than spines but, because the number of TH-labeled varicosities observed in synaptic junctions was so small, it was not deemed proper to number their relative proportions. Both synaptic configurations were observed in each region, at both ages and in control as well as cKO mice, except in the NAC of adult control and cKO mice, two samples in which only a single varicosity was found to engage in a structurally identifiable synapse (with a dendritic branch). In neostriatum, two examples of synapses on the neck of spines were seen, including the one illustrated in Fig. 4A. This particular TH-labeled varicosity was most unusual in making two synapses with different dendritic branches.

As illustrated in Fig. 5, the 115 TH-labeled axon terminals examined in the NAC of adult wild-type mice perfused with a mixture of glutaraldehyde and formaldehyde did not differ in any

FIG. 5. DA terminals from the core of nucleus accumbens in adult wild-type mice fixed by perfusion with a glutaraldehyde–paraformaldehyde mixture. There was no apparent difference in the ultrastructural features of TH-labeled varicosities from these mice, by comparison with those from control and cKO mice perfused with acrolein as primary fixative (see Results for morphometric data). (A and A') Two sections across the same labeled varicosity, which forms a relatively wide symmetrical synaptic contact (between small arrows) with a dendritic branch (db). (B) Two labeled varicosity profiles appear more typically asymmetrical. Scale bar (in B), 1  $\mu\text{m}$ .

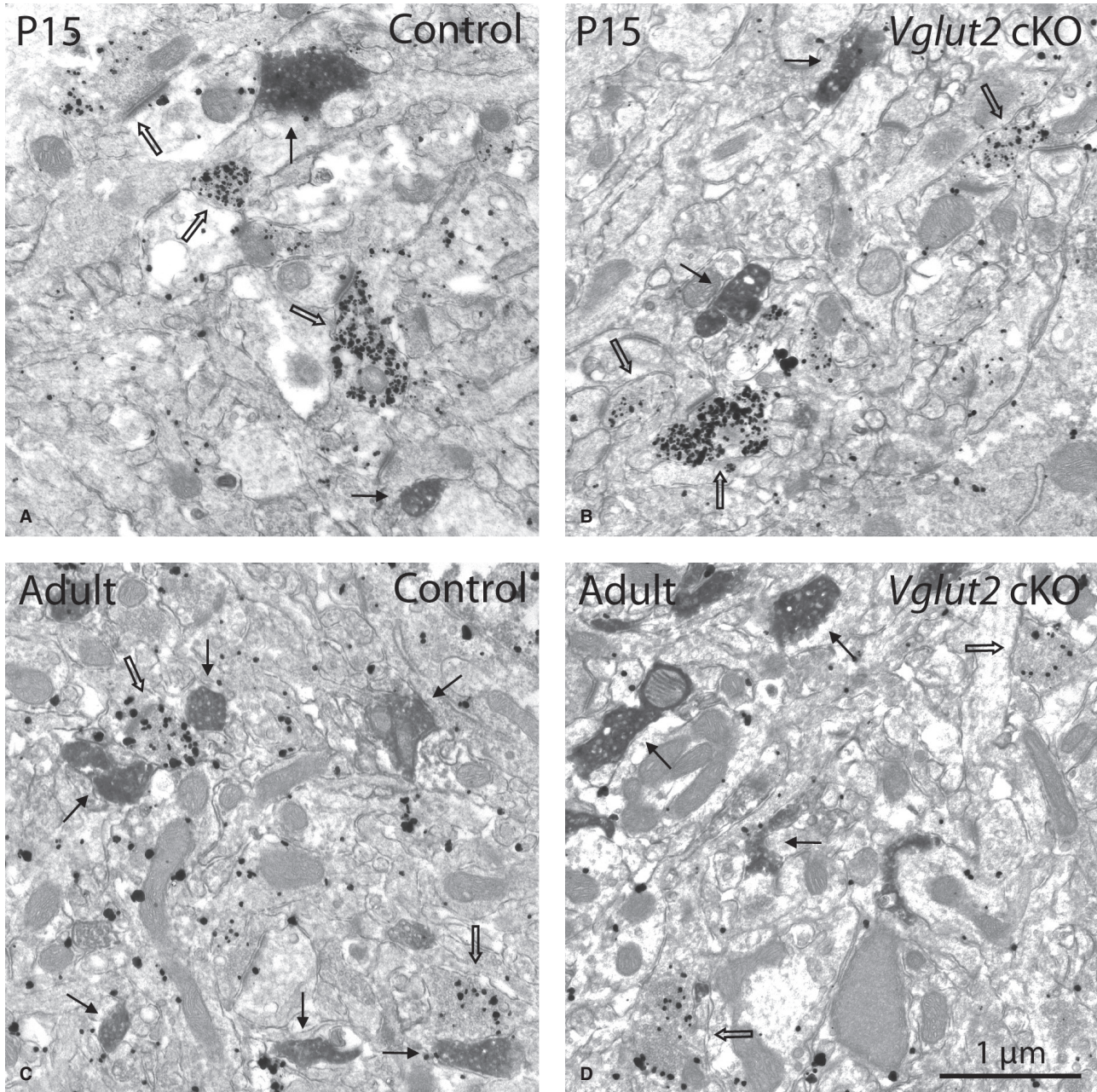


FIG. 6. Low-magnification electron micrographs illustrating the lack of dually TH-VGLUT2-labeled axon terminals in control as well as cKO mice. (A and B) From the NAC and NAS of P15 mice; (C and D) from the NS of adult mice. TH and VGLUT2 were respectively labeled with the immunoperoxidase technique (fine diamminobenzidine precipitate) and the immunogold technique (silver-intensified immunogold particles). TH terminals are designated by solid arrows and VGLUT2 terminals by open arrows. Scale bar (in D), 1  $\mu\text{m}$ .

way from those perfused with acrolein as primary fixative (average diameter,  $0.46 \pm 0.01 \mu\text{m}$ ; area,  $0.17 \pm 0.01 \mu\text{m}^2$ ; percentage with mitochondria,  $34 \pm 5\%$ ; average length of junctions,  $0.19 \pm 0.04 \mu\text{m}$ ; frequency of synaptic junction in single thin sections,  $3 \pm 1\%$ ).

#### *Lack of dually TH-VGLUT2-immunolabeled axon varicosities in mouse ventral and dorsal striatum*

As shown in Table S1 and illustrated in Fig. 6, a large number of TH- or VGLUT2-immunolabeled axon terminals could be observed in

the electron microscopic material prepared for dual immunolabeling. Despite this extensive examination, however, not a single axon terminal was found to be convincingly dually labeled in either region of the control or of the cKO mice, of either age.

#### Discussion

The main finding of the present study is that DA (TH-labeled) axon varicosities in the ventral and dorsal mouse striatum are very rarely synaptic. This was observed in both immature and mature cKO and control animals, as well as in wild-type adults.

### Methodological considerations

The anatomical distribution of the immunocytochemical labeling obtained with the present TH antibody confirmed its specificity, as established in earlier studies (for example, see Kawano *et al.*, 2006). In theory, TH immunoreactivity should identify noradrenaline as well as DA axon terminals in the striatum, but the latter are known to be scarce in NS and only slightly more common in NAC and NAS (Carlsson, 1959; Moore & Card, 1984).

Because the present electron microscopic analysis was carried out in single rather than serial thin sections, there was a risk of underestimating the frequency with which the TH-labeled terminals made a synaptic membrane specialization, especially after labeling with the immunoperoxidase–DAB technique. This was the reason for keeping the density of DAB immunoprecipitate to a level ensuring clearcut detection, but which did not occlude eventual areas of synaptic membrane differentiation. However, all observed junctional complexes made by TH-labeled varicosities were relatively small, usually symmetrical and often poorly differentiated. For this reason, and knowing how much synaptic junctions can vary in their amount of postsynaptic opacity (see Colonnier, 1968), mere localized straightenings of apposed membrane were accepted as evidence of a junction (e.g. Figs 2D, 3A and 5A,A').

In the search for dually labeled terminals there was no reason to doubt the double immunolabeling method used, as it had consistently provided positive results in the rat and had revealed the expected high number of varicosity profiles immunolabeled for either TH and VGLUT2 in the mouse. As in our previous studies, VGLUT2 was detected with the immunogold and TH with the immunoperoxidase technique, to allow for comparison between double labeling and earlier or present single labeling data. The double immunolabeling was carried out in that order, because artefactual immunogold deposits over all TH-positive terminals had been found in prior experiments carried out in the reverse order.

### Intrinsic and relational features of striatal DA terminals

To our knowledge, this is the first extensive description of the ultrastructural characteristics of DA (TH-immunolabeled) axon terminal arborizations in ventral as well as dorsal striatum of the mouse. Triarhou *et al.* (1988) provided some information about the relationships of TH-labeled varicosities in the dorsolateral striatum (but not the NAC or NAS), and it was not clear whether the single-section profiles of these varicosities had been systematically examined to estimate synaptic incidence. The relatively high synaptic frequency then reported for two wild-type mice (27%) should therefore be regarded with caution.

The small average size of mesostriatal DA varicosities measured in the present study was consistent with earlier measurements made in rat by electron microscopic [<sup>3</sup>H]DA uptake autoradiography (Descarries *et al.*, 1996) or TH immunocytochemistry (Pickel *et al.*, 1981; Freund *et al.*, 1984; Voorn *et al.*, 1986; Zahm, 1992; Descarries *et al.*, 1996; Bérubé-Carrière *et al.*, 2009). The sole exception was the study by Antonopoulos *et al.* (2002) during postnatal rat development, in which an almost twice as large average size of TH-labeled varicosity profiles was reported (0.8–0.9  $\mu$ m in diameter). This presumably reflected a sampling bias and could account for the exceedingly high values of synaptic incidence (80–100%) which were then extrapolated using the stereological formula of Beaudet & Sotelo (1981). The equivalent average size of striatal DA varicosities at P15 and in the adult had already been noted in our previous study in the rat (Bérubé-Carrière *et al.*, 2009). If the size of axon terminals somehow relates to their physiological strength (Pierce & Lewin, 1994), this could indicate that

these terminals are fully functional at P15. Likewise, the percentage of varicosity profiles exhibiting mitochondria was similar in all subgroups, suggesting similar energetic demands.

The very low frequency of synaptic striatal DA varicosities observed in the NAC, NAS and NS of P15 and adult mice was suggestive of a species difference between mice and rats, in the latter of which previous measurements have yielded significantly higher proportions. Zahm (1992) had reported percentages of 2.3–2.9% in a large systematic sample of TH-labeled varicosities from NAC, NAS and NS, but this was in single thin sections and not extrapolated to the whole volume of varicosities. In our own study after double TH and VGLUT2 immunolabeling, the values of synaptic incidence extrapolated to the whole volume of TH-labeled varicosities were 55 and 31% in the NAC and NS of P15 rats, and 7 and 6% in the NAC and NS of adult rats, respectively (Bérubé-Carrière *et al.*, 2009). As repeatedly observed in rat, most of the rare junctional DA varicosities in mouse striatum made symmetrical synapses with dendritic branches. Strategic synaptic localizations such as the neck of spines (e.g., Freund *et al.*, 1984; Descarries *et al.*, 1996) were very rare in the mouse.

It was unexpected not to find a single axon terminal dually immunolabeled for both TH and VGLUT2 in either the nucleus accumbens or the neostriatum of P15 and adult control mice. It is tempting to speculate that this finding is indicative of an earlier regression of the dual DA–glutamate phenotype with maturation in mice than rats. This results, however, needs to be reconciled with recent optogenetic findings, obtained in brain slices from adult mice, which demonstrate that selective stimulation of DA neurons of the VTA may evoke glutamatergic synaptic events in the NAs (Stuber *et al.*, 2010; Tecuapetla *et al.*, 2010). Several explanations have already been proposed for such a discrepancy (Moss *et al.*, 2011), among which the most interesting could be an early segregation of TH and VGLUT2 in distinct axon terminals of mesostriatal DA neurons (Trudeau, 2004; El Mestikawy *et al.*, 2011). Such a fundamental issue will obviously need to be addressed in future experiments.

Interestingly, the synaptic incidence of striatal DA varicosities as well as their size and the proportion containing mitochondria were similar in the two cKO mouse lines and their littermate controls. In another study carried out in parallel, an approximately 20% reduction in the number of DA neurons was recently documented in the ventral mesencephalon of the Mtl *Vglut2* cKO mice, accounting for a reduced density of DA innervation (approximately 30%) and diminished DA release in the nucleus accumbens of these mice (G.M. Fortin, M.J. Bourque, J.A. Mendez, D. Leo, K. Nordenankar, C. Birgner, E. Arvidsson, V.V. Rymar, N. Bérubé-Carrière, L. Descarries, A.F. Sadikot, Å. Wallén-Mackenzie & L.É. Trudeau, unpublished data). Furthermore, *in vitro*, the growth and survival of cultured DA neurons from these cKO mice was then shown to be impaired. Taken together, these observations suggest that the dual glutamate–DA phenotype of mesencephalic DA neurons, which is particularly prominent during development, could be more important for regulating the number and growth of these neurons than for their establishment and/or maintenance of a scarce synaptic connectivity.

### A new image of the mesostriatal DA innervation

Even if a definitive description of the mesostriatal DA innervation in the mouse awaits its three-dimensional reconstruction at the electron microscopic level, the present examination in single thin sections justifies a revision of preconceived notions on the morphological organization of this system. In rat, nigrostriatal DA axons have been shown to project directly to, and branch profusely within, striatum

(Gauthier *et al.*, 1999; see also Prensa & Parent, 2001), giving rise to a very dense innervation, estimated at  $1 \times 10^8$  varicosities per  $\text{mm}^3$  in the striatal matrix and  $1.7 \times 10^8$  in the striosomes and subcallosal streak (Doucet *et al.*, 1986). As visualized with a viral vector expressing membrane-targeted green fluorescent protein, single mesostriatal DA axons form an extremely profuse, bush-like terminal arbour extending over a relatively large striatal volume (Matsuda *et al.*, 2009). At the ultrastructural level, the frequent proximity and occasional juxtaposition of TH-labeled varicosity profiles reflects this density of innervation (e.g. fig. 3 in Descarries *et al.*, 1996). It is also apparent that, in all parts of striatum, many DA varicosities may be continuous along the same axon rather than spaced at intervals of a few microns, as is the case with its less dense serotonin innervation, for example (e.g., Soghomonian *et al.*, 1987, 1989). Also meaningful is the presence of synaptic vesicle aggregates within narrow as well as enlarged segments of the DA axons (e.g., Freund *et al.*, 1984; Voorn *et al.*, 1986), which suggests that exocytotic DA release might occur along the whole extent of these axonal arborizations rather than only at their sites of varicose dilation.

### Functional considerations

Because such a small proportion of striatal DA varicosities form differentiated synaptic junctions in the mouse, it may also be inferred that diffuse transmission plays a particularly important role in the functioning of the mesostriatal system in this species. How this relates to specific functions and behaviors controlled by the DA system in mouse as opposed to other rodents and more phylogenetically distant species such as primates and humans remains to be determined. The extreme density of the mesostriatal DA innervation and the possible diffusion of DA in the extracellular space despite DA reuptake (Wightman & Zimmerman, 1990) has also led to us to postulate that spontaneous and evoked release from such a multitude of release sites permanently maintains a low basal extracellular level of DA throughout the striatum (Descarries *et al.*, 1996). Several studies have indeed demonstrated that there are physiologically relevant basal concentrations of DA in the rat striatal neuropil (Parsons & Justice, 1992), upon which DA efflux occurring in response to single action potentials or burst firing will be superimposed (Garris *et al.*, 1994; Zhang *et al.*, 2009). Among other functions, this ambient level of DA could allow for a sustained activation and regulation of the widely distributed high-affinity receptors for DA and/or other transmitters in striatum. The fact that only a low level of DA would be needed to maintain such a control might in turn account for the notion that a large proportion of DA terminals must be lost before clinical manifestations result from lesions of the mesostriatal system, and for restoration of its functioning by grafts of DA neurons (Perlow *et al.*, 1979) that do not reestablish the pre-existent synaptic circuitry.

### Supporting Information

Additional supporting information can be found in the online version of this article:

Table S1. Surface of thin section examined ( $\mu\text{m}^2$ ) and number of TH and VGLUT2 terminals visualized after dual TH/VGLUT2 immunolabeling.

Table S2. DA axon terminals in the nucleus accumbens (core and shell) and neostriatum of immature (P15) and mature (P70-90) mice of the two lines of *Vglut2* cKO (Upp and Mtl).

Table S3. DA axon terminals in the nucleus accumbens (core and shell) and neostriatum of immature (P15) and mature (P70-90) littermate control mice for the two lines of *Vglut2* cKO (Upp and Mtl).

Table S4. *P* values for *t*-tests of Control vs. cKO mice.

Please note: As a service to our authors and readers, this journal provides supporting information supplied by the authors. Such materials are peer-reviewed and may be re-organized for online delivery, but are not copy-edited or typeset by Wiley-Blackwell. Technical support issues arising from supporting information (other than missing files) should be addressed to the authors.

### Acknowledgements

N.B.-C. was the recipient of a doctoral studentship from the Fonds de la Recherche en Santé du Québec (FRSQ). This work was funded in part by CIHR grants MOP-3544 and MOP-106562 to L.D., MOP-49951 to L.-É.T., and MOP-106556 to L.-É.T. and L.D., as well a grant from NARSAD to L.-É.T. L.-É.T. and L.D. also benefitted from an infrastructure grant of the FRSQ to the GRSNC (Groupe de Recherche sur le Système Nerveux Central), and L.-É.T. and Å.W.-M. from a joint grant of The Swedish Foundation for International Cooperation in Research and Higher Education. Research in Å.W.-M.'s laboratory is supported by the Swedish Research Council, the Swedish Brain Foundation, Swedish Brain Power, the Åhlén and Wiberg Foundations, the National Board of Health and Welfare and Uppsala University. Karin Nordenankar and Diane Gingras provided technical assistance. The authors also thank Professor Nils-Göran Larsson for sharing the DAT-Cre mouse line at the origin of the Uppsala *Vglut2<sup>f/f</sup>/f<sup>DAT-cre</sup>* mouse, and Drs Xiaoxi Zhuang and Bradford Lowell for having produced and provided the mice at the origin of the Montreal *Vglut2<sup>f/f</sup>/f<sup>DAT-cre</sup>* mouse.

### Abbreviations

cKO, conditional knockout; CNS, central nervous system; DA, dopamine; DAB, 3,3'-diaminobenzidine tetrahydrochloride; Mtl, mice generated in Montreal; NAC, nucleus accumbens core; NAS, nucleus accumbens shell; NS, neostriatum; TH, tyrosine hydroxylase; Upp, mice generated in Uppsala; VGLUT2, type 2 vesicular glutamate transporter.

### References

- Antonopoulos, J., Dori, I., Dinopoulos, A., Chiotelli, M. & Parnavelas, J.G. (2002) Postnatal development of the dopaminergic system of the striatum in the rat. *Neuroscience*, **110**, 245–256.
- Beaudet, A. & Descarries, L. (1976) Quantitative data on serotonin nerve terminals in adult rat neocortex. *Brain Res.*, **111**, 301–309.
- Beaudet, A. & Sotelo, C. (1981) Synaptic remodeling of serotonin axon terminals in rat agranular cerebellum. *Brain Res.*, **206**, 305–329.
- Bérubé-Carrière, N., Riad, M., Dal Bo, G., Lévesque, D., Trudeau, L.-É. & Descarries, L. (2009) The dual dopamine-glutamate phenotype of growing mesencephalic neurons regresses in mature rat brain. *J. Comp. Neurol.*, **517**, 873–891.
- Birgner, C., Nordenankar, K., Lundblad, M., Mendez, J.A., Smith, C., le Greves, M., Galter, D., Olson, L., Fredriksson, A., Trudeau, L.-É., Kullander, K. & Wallén-Mackenzie, Å. (2009) VGLUT2 in dopamine neurons is required for psychostimulant-induced behavioral activation. *Proc. Natl. Acad. Sci. USA*, **107**, 389–394.
- Carlsson, A. (1959) The occurrence, distribution and physiological role of catecholamines in the nervous system. *Pharmacol. Rev.*, **11**, 490–493.
- Colonnier, M. (1968) Synaptic patterns on different cell types in the different laminae of the cat visual cortex. An electron microscope study. *Brain Res.*, **9**, 268–287.
- Dal Bo, G., St-Gelais, F., Danik, M., Williams, S., Cotton, M. & Trudeau, L.-É. (2004) Dopamine neurons in culture express VGLUT2 explaining their capacity to release glutamate at synapses in addition to dopamine. *J. Neurochem.*, **88**, 1398–1405.
- Dal Bo, G., Bérubé-Carrière, N., Mendez, J.A., Leo, D., Riad, M., Descarries, L., Lévesque, D. & Trudeau, L.-É. (2008) Enhanced glutamatergic phenotype of mesencephalic dopamine neurons after neonatal 6-hydroxy-dopamine lesion. *Neuroscience*, **156**, 59–70.
- Descarries, L., Beaudet, A. & Watkins, K.C. (1975) Serotonin nerve terminals in adult rat neocortex. *Brain Res.*, **100**, 563–588.
- Descarries, L., Watkins, K.C. & Lapierre, Y. (1977) Noradrenergic axon terminals in the cerebral cortex of rat. III. Topometric ultrastructural analysis. *Brain Res.*, **133**, 197–222.

- Descarries, L., Watkins, K.C., Garcia, S., Bosler, O. & Doucet, G. (1996) Dual character, asynaptic and synaptic, of the dopamine innervation in adult rat neostriatum: a quantitative autoradiographic and immunocytochemical analysis. *J. Comp. Neurol.*, **375**, 167–186.
- Descarries, L., Bérubé-Carrière, N., Riad, M., Bo, G.D., Mendez, J.A. & Trudeau, L.-É. (2008) Glutamate in dopamine neurons: synaptic versus diffuse transmission. *Brain Res. Rev.*, **58**, 290–302.
- Doucet, G., Descarries, L. & Garcia, S. (1986) Quantification of the dopamine innervation in adult rat neostriatum. *Neuroscience*, **19**, 427–445.
- Ekstrand, M.I., Terzioglu, M., Galter, D., Zhu, S., Hofstetter, C., Lindqvist, E., Thams, S., Bergstrand, A., Hansson, F.S., Trifunovic, A., Hoffer, B., Cullheim, S., Mohammed, A.H., Olson, L. & Larsson, N.G. (2007) Progressive parkinsonism in mice with respiratory-chain-deficient dopamine neurons. *Proc. Natl. Acad. Sci. USA*, **104**, 1325–1330.
- El Mestikawy, S., Wallén-Mackenzie, A., Fortin, G.M., Descarries, L. & Trudeau, L.-É. (2011) From glutamate co-release to vesicular synergy: vesicular glutamate transporters. *Nat. Rev. Neurosci.*, **12**, 204–216.
- Franklin, K.B.J. & Paxinos, G. (2008) *The Mouse Brain in Stereotaxic Coordinates*. Elsevier Academic Press, New York.
- Freund, T.F., Powell, J.F. & Smith, A.D. (1984) Tyrosine hydroxylase-immunoreactive boutons in synaptic contact with identified striatonigral neurons, with particular reference to dendritic spines. *Neuroscience*, **13**, 1189–1215.
- Garris, P.A., Ciolkowski, E.L., Pastore, P. & Wightman, R.M. (1994) Efflux of dopamine from the synaptic cleft in the nucleus accumbens of the rat brain. *J. Neurosci.*, **14**, 6084–6093.
- Gauthier, J., Parent, M., Lévesque, M. & Parent, A. (1999) The axonal arborization of single nigrostriatal neurons in rats. *Brain Res.*, **834**, 228–232.
- Haycock, J.W. (1993) Multiple forms of tyrosine hydroxylase in human neuroblastoma cells: quantitation with isoform-specific antibodies. *J. Neurochem.*, **60**, 493–502.
- Kawano, M., Kawasaki, A., Sakata-Haga, H., Fukui, Y., Kawano, H., Nogami, H. & Hisano, S. (2006) Particular subpopulations of midbrain and hypothalamic dopamine neurons express vesicular glutamate transporter 2 in the rat brain. *J. Comp. Neurol.*, **498**, 581–592.
- Matsuda, W., Furuta, T., Nakamura, K.C., Hioki, H., Fujiyama, F., Arai, R. & Kaneko, T. (2009) Single nigrostriatal dopaminergic neurons form widely spread and highly dense axonal arborizations in the neostriatum. *J. Neurosci.*, **29**, 444–453.
- Mendez, J.A., Bourque, M.J., Dal Bo, G., Bourdeau, M.L., Danik, M., Williams, S., Lacaille, J.C. & Trudeau, L.-É. (2008) Developmental and target-dependent regulation of vesicular glutamate transporter expression by dopamine neurons. *J. Neurosci.*, **28**, 6309–6318.
- Moore, R.Y. & Card, J.P. (1984) Noradrenaline-containing neuron systems. In Björklund, A. & Hökfelt, T. (Eds), *Handbook of Chemical Neuroanatomy*. Elsevier, Amsterdam, pp. 123–156.
- Moss, J., Ungless, M.A. & Bolam, J.P. (2011) Dopaminergic axons in different divisions of the adult rat striatal complex do not express vesicular glutamate transporters. *Eur. J. Neurosci.*, **33**, 1205–1211.
- Palade, G.E. & Palay, S.L. (1954) Electron microscope observations of interneuronal and neuromuscular synapses. *Anat. Rec.*, **118**, 335–336.
- Parsons, L.H. & Justice, J.B. Jr (1992) Extracellular concentration and in vivo recovery of dopamine in the nucleus accumbens using microdialysis. *J. Neurochem.*, **58**, 212–218.
- Perlow, M.J., Freed, W.J., Hoffer, B.J., Seiger, A., Olson, L. & Wyatt, R.J. (1979) Brain grafts reduce motor abnormalities produced by destruction of nigrostriatal dopamine system. *Science*, **204**, 643–647.
- Persson, S., Boulland, J.L., Aspling, M., Larsson, M., Freneau, R.T. Jr, Edwards, R.H., Storm-Mathisen, J., Chaudhry, F.A. & Broman, J. (2006) Distribution of vesicular glutamate transporters 1 and 2 in the rat spinal cord, with a note on the spinocervical tract. *J. Comp. Neurol.*, **497**, 683–701.
- Peters, A. & Palay, S.L. (1996) The morphology of synapses. *J. Neurocytol.*, **25**, 687–700.
- Pickel, V.M., Beckley, S.C., Joh, T.H. & Reis, D.J. (1981) Ultrastructural immunocytochemical localization of tyrosine hydroxylase in the neostriatum. *Brain Res.*, **225**, 373–385.
- Pierce, J.P. & Lewin, G.R. (1994) An ultrastructural size principle. *Neuroscience*, **58**, 441–446.
- Prensa, L. & Parent, A. (2001) The nigrostriatal pathway in the rat: a single-axon study of the relationship between dorsal and ventral tier nigral neurons and the striosome/matrix striatal compartments. *J. Neurosci.*, **21**, 7247–7260.
- Robertson, J.D. (1953) Ultrastructure of two invertebrate synapses. *Proc. Soc. Exp. Biol. Med.*, **82**, 219–223.
- Sherrington, C.S. (1897) The central nervous system. In Foster, M. & Sherrington, C.S. (Eds), *A Textbook of Physiology*. Macmillan, London, pp. 915–1000.
- Soghomonian, J.J., Doucet, G. & Descarries, L. (1987) Serotonin innervation in adult rat neostriatum. I. Quantified regional distribution. *Brain Res.*, **425**, 85–100.
- Soghomonian, J.J., Descarries, L. & Watkins, K.C. (1989) Serotonin innervation in adult rat neostriatum. II. Ultrastructural features: a radioautographic and immunocytochemical study. *Brain Res.*, **481**, 67–86.
- Stuber, G.D., Hnasko, T.S., Britt, J.P., Edwards, R.H. & Bonci, A. (2010) Dopaminergic terminals in the nucleus accumbens but not the dorsal striatum corelease glutamate. *J. Neurosci.*, **30**, 8229–8233.
- Takamori, S., Rhee, J.S., Rosenmund, C. & Jahn, R. (2001) Identification of differentiation-associated brain-specific phosphate transporter as a second vesicular glutamate transporter (VGLUT2). *J. Neurosci.*, **21**, RC182.
- Tecuapetla, F., Patel, J.C., Xenias, H., English, D., Tadros, I., Shah, F., Berlin, J., Deisseroth, K., Rice, M.E., Tepper, J.M. & Koos, T. (2010) Glutamatergic signaling by mesolimbic dopamine neurons in the nucleus accumbens. *J. Neurosci.*, **30**, 7105–7110.
- Tong, Q., Ye, C., McCrimmon, R.J., Dhillon, H., Choi, B., Kramer, M.D., Yu, J., Yang, Z., Christiansen, L.M., Lee, C.E., Choi, C.S., Zigman, J.M., Shulman, G.I., Sherwin, R.S., Elmquist, J.K. & Lowell, B.B. (2007) Synaptic glutamate release by ventromedial hypothalamic neurons is part of the neurocircuitry that prevents hypoglycemia. *Cell Metab.*, **5**, 383–393.
- Triarhou, L.C., Norton, J. & Ghetti, B. (1988) Synaptic connectivity of tyrosine hydroxylase immunoreactive nerve terminals in the striatum of normal, heterozygous and homozygous weaver mutant mice. *J. Neurocytol.*, **17**, 221–232.
- Trudeau, L.-É. (2004) Glutamate co-transmission as an emerging concept in monoamine neuron function. *J. Psychiatry Neurosci.*, **29**, 296–310.
- Voorn, P., Jorritsma-Byham, B., Van Dijk, C. & Buijs, R.M. (1986) The dopaminergic innervation of the ventral striatum in the rat: a light- and electron-microscopical study with antibodies against dopamine. *J. Comp. Neurol.*, **251**, 84–99.
- Wallén-Mackenzie, Å., Gezelius, H., Thoby-Brisson, M., Nygard, A., Enjin, A., Fujiyama, F., Fortin, G. & Kullander, K. (2006) Vesicular glutamate transporter 2 is required for central respiratory rhythm generation but not for locomotor central pattern generation. *J. Neurosci.*, **26**, 12294–12307.
- Wightman, R.M. & Zimmerman, J.B. (1990) Control of dopamine extracellular concentration in rat striatum by impulse flow and uptake. *Brain Res. Brain Res. Rev.*, **15**, 135–144.
- Yamaguchi, T., Sheen, W. & Morales, M. (2007) Glutamatergic neurons are present in the rat ventral tegmental area. *Eur. J. Neurosci.*, **25**, 106–118.
- Zahm, D.S. (1992) An electron microscopic morphometric comparison of tyrosine hydroxylase immunoreactive innervation in the neostriatum and the nucleus accumbens core and shell. *Brain Res.*, **575**, 341–346.
- Zhang, L., Doyon, W.M., Clark, J.J., Phillips, P.E. & Dani, J.A. (2009) Controls of tonic and phasic dopamine transmission in the dorsal and ventral striatum. *Mol. Pharmacol.*, **76**, 396–404.
- Zhou, J., Nannapaneni, N. & Shore, S. (2007) Vesicular glutamate transporters 1 and 2 are differentially associated with auditory nerve and spinal trigeminal inputs to the cochlear nucleus. *J. Comp. Neurol.*, **500**, 777–787.
- Zhuang, X., Masson, J., Gingrich, J.A., Rayport, S. & Hen, R. (2005) Targeted gene expression in dopamine and serotonin neurons of the mouse brain. *J. Neurosci. Methods*, **143**, 27–32.